Spectrochimica Acta Part A: Molecular and Biomolecular Spectroscopy 351 (2026) 127509

Contents lists available at ScienceDirect

Spectrochimica Acta Part A:
Molecular and Biomolecular Spectroscopy

journal homepage: www.journals.elsevier.com/spectrochimica-acta-part-a-molecular-and-biomolecular-spectroscopy

Exploring the use of FTIR Amide I band deconvolution to investigate protein secondary structure and texturisation during high moisture extrusion

Clara Barnés-Calle [a], Pere Gou [a], Elena Fulladosa [a,*], Frans W.J. van den Berg [b]

[a] IRTA. Food Quality and Technology. Finca Camps i Armet, s/n, 17121 Monells, Girona, Spain
[b] Department of Food Science, University of Copenhagen, Frederiksberg, Denmark

HIGHLIGHTS

- High moisture extrusion processing (HMEP) texturizes plant-based protein sources.
- Protein secondary structure changes can be detected via FTIR amide I band analysis.
- FTIR Amide *I* band deconvolution critically depends on the analytical procedure used.
- HMEP changes protein secondary structure of fava bean protein concentrate (FBPC).
- Secondary protein structure did not explain texturisation level of FBPC extrudates.

GRAPHICAL ABSTRACT

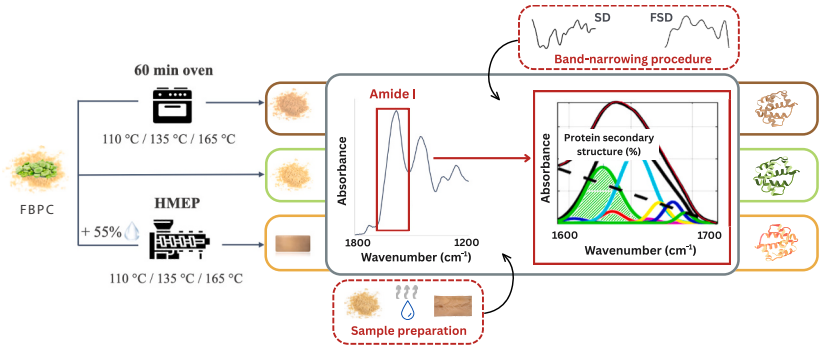

ARTICLE INFO

Keywords:
Fava bean
Meat analogues
Fourier-transform infrared spectroscopy
Amide I band
Protein structure
Anisotropy index

ABSTRACT

Fourier transform infrared spectroscopy (FTIR) combined with Amide I band deconvolution has been used to investigate protein structural changes occurring during high moisture extrusion processing (HMEP). However, it is a sensitive, user-dependent technique that has sparked debate over its appropriate analytical approach. This paper aims to assess the suitability of FTIR Amide *I* band deconvolution to investigate protein structural changes in fava bean protein concentrate (FBPC) caused by temperature treatment and/or HMEP at different temperatures (110 °C, 135 °C and 165 °C), and to explore its relationship with the texturisation level of the obtained products. Influence of sample preparation and parameter selection during FTIR deconvolution procedure was also explored. To do so, FBPC was heated in a convection oven or subjected to HMEP at different temperatures (110, 135 or 165 °C), and Fourier self-deconvolution (FSD) and second derivative (SD) were explored as band-narrowing methods to analyse protein conformation from FTIR spectra. FTIR Amide I band deconvolution showed high sensitivity to sample preparation and parameter selection during FSD and SD analytical procedure. Results suggested that HMEP caused the denaturation of β-sheet forms present initially in FBPC, and an increase of other structures including intermolecular β-sheet and/or aggregates—probably due to the formation of new intermolecular bonds. Moreover, although higher temperature during HMEP enhanced fibre-like structure formation, texturisation level could not be directly related to the protein conformation of the final high moisture

* Corresponding author.
E-mail address: elena.fulladosa@irta.cat (E. Fulladosa).

https://doi.org/10.1016/j.saa.2026.127509
Received 2 October 2025; Received in revised form 23 December 2025; Accepted 19 January 2026
Available online 21 January 2026

extrudates (HME), since no significant differences were observed between protein secondary structure of HME under the studied conditions.

1. Introduction

High moisture extrusion processing (HMEP) is gaining interest for its potential to improve the fibrous texture of meat analogues derived from alternative protein sources. Soy, pea and wheat have been the most used protein sources to produce meat alternatives [1]. Other sources such as fava bean have also shown potential as future sustainable protein supplies [2], and fibrous structures from fava bean protein concentrate (FBPC) by means of HMEP have been obtained in previous studies [3,4]. High temperatures, shear force and pressure applied during HMEP cause proteins to unfold, aggregate and realign [5], allowing for the formation of fibrous structures during the cooling stage. However, to date, the effect of HMEP on texturization, protein dissociation and molecular realignment is poorly understood and often described as being a "black box" [6].

Fourier Transform Infrared Spectroscopy (FTIR) has been widely used to study the structure of different alternative protein sources including yeast, pulses and cereals [7–9], and has been recently investigated as a tool to study the effect of HMEP on secondary protein structure [10–12]. Protein molecules encompass vibrational coupling caused by electrostatic interactions between the transition dipoles of individual amide vibrations, and are determined by their three-dimensional structure and its vibrational force field [13]. Therefore, their vibrational spectrum can provide information on the structure and on intramolecular and intermolecular interactions, which can be correlated with specific secondary structural folds such as α-helices and β-sheets. In this context, nine characteristic group frequencies known as amide bands—named Amide A, B, I, II…VII—have been identified [14], being Amide I (~1650 cm^{-1}) and Amide II (~1550 cm^{-1}) regions the two major bands in the protein IR spectrum [15]. Less frequently, the Amide III region (~1300 cm^{-1}) has also been used to investigate protein structure of food matrices [16–18].

In the Amide *I* region, the vibrations are primarily caused by C═O stretching mode mixed with other minor contributions—such as C—N stretching and N—H bending—and show significant coupling due to its large transitional dipole moment [13]. It is the most commonly studied for this purpose as it is the most sensitive spectral range to protein secondary structure compositions [15]. These structures are present as individual bands that overlap forming a broader spectral feature and require mathematical band-narrowing procedures such as second-derivative (SD) and Fourier self-deconvolution (FSD) to be identified [19]. Although band assignments can be based on one or the other [20], precautions are needed to distinguish real hidden peaks. On one hand, derivatives are especially sensitive to noise in the original spectrum and can be distorted by edge effects and, on the other hand, FSD can be affected by noise or water vapor producing new peaks that are not real [21–23]. Calculating both SD and FSD and only considering bands visible by both techniques may thus help reduce artifacts introduced by data processing [21] and have been used complementarily in numerous recent publications regarding FTIR Amide *I* deconvolution of spectra from high moisture extrudates (HME) [24]. Once the number of hidden peaks has been identified, curve fitting procedures based on iterative adjustments of heights, widths and position parameters in a mathematical model of the individual absorbance bands allow for the quantification of secondary protein structures in a given food product [25].

The use of these techniques for the identification of changes in protein secondary structure caused by the short-time high temperatures, pressure and shear stress involved in HMEP could help elucidate the role of protein structuring during the texturization process, as well as giving information on nutritional aspects of the final product in terms of digestibility [7]. However, there seems to be a lack of agreement on the proper analytical pathway of FTIR Amide I band deconvolution where critical steps such as selection of filter thresholds [26] can lead to significant deviations from the real spectrum, and thus to substantial differences in quantification. At the same time, mathematically, the curve-fitting analysis of amide bands contains an element of subjectivity (choice of input parameters) and uncertainty [27]. These limitations have caused inconsistencies across studies and no clear consensus on protein secondary structure evolution during HMEP up to now [24], which raises questions on the ambiguity of data interpretation.

The objective of this study was to assess the suitability of FTIR Amide I band deconvolution for the examination of protein structural changes in fava bean protein concentrate caused by temperature and/or HMEP, and its relationship with the texturisation level of the obtained HME. The influence of sample preparation and parameter selection during FTIR deconvolution procedure on the protein secondary structure determinations was also explored.

2. Materials and methods

2.1. Raw materials

Deflavoured fava bean protein concentrate (FBPC) (FFBP-60-D, AGT Food and Ingredients, Minot, ND, USA), with 60.4% of protein content on dry basis, was used to explore the effect of temperature treatment on protein secondary structure. FBPC and bottled water (Font Vella, Aguas Danone SA, Spain) were used to produce HME samples at different conditions to study the effect of HMEP on protein secondary structure and texturization.

2.2. Sample treatments

2.2.1. Thermal treatment of FBPC

FBPC powder was thermally treated at different conditions to study the effect of temperature on the secondary protein structures. Samples of approximately 100 g of powder were weighed in metallic vessels and put in a convection oven (300 plus series, Gallenkamp, Cambridge, UK) at different temperatures (110, 135 or 165 °C) for 60 min. After the treatment, samples were placed in a desiccator over silica gel (Aldrich ® Essentials, Sigma-Aldrich, Merck Group, Missouri, USA) and cooled to room temperature before further analysis.

2.2.2. Production of fava bean HME at different conditions

FBPC-based HME samples were produced using a laboratory-scale co-rotating and intermeshing twin-screw extruder (Process 11, Thermo Fisher Scientific Inc., Waltham, MA, USA). The extruder was equipped with a peristaltic pump (Reglo ICC Pump, ISMATEC, IDEX Health and Science LLC, Oak Harbor, WA, USA) and a vertical Volumetric MiniTwin Feeder with agitator (Brabender Technology GmbH, Duisburg, Germany) to feed water and protein powder, respectively. A cooling die (H 4 mm x W 19 mm x L 125 mm) supplied by a refrigerated bath circulator ("KISS K6", HUBER, Peter Huber Kältemaschinenban AG, Offenburg, Germany) set at 20 °C was assembled at the end of the extruder outlet.

During the extrusion process, screw speed was set at 650 rpm and temperatures in heating zones Z2 to Z4 were fixed at 50, 90 and 110 °C, and the die zone at 100 °C, as described in a previous work [28]. Water and protein feed was 55% and 45%, respectively, at a total feeding rate of 12 g/min. The temperature in heating zones Z5 to Z8 were modified in the range of 110 °C to 165 °C (110 °C, 135 °C or 165 °C). For each extrusion temperature, three independent batches of samples were produced. All samples were manually cut and collected, sealed in plastic bags, and stored at −18 ± 2 °C until further analysis. Prior to analysis,

samples were thawed at 4 °C overnight.

2.3. Attenuated total reflectance FTIR analysis procedure

2.3.1. Sample preparation

All samples (raw FBPC, thermally treated FBPC and frozen HME samples (−18 ± 2 °C)) were stored at −80 °C for at least 2 h and transferred to a vacuum freeze dryer (LyoMicron Freeze dryer, Coolvacuum Technologies, Barcelona, Spain) equipped with a condenser set at −40 °C. All samples were freeze-dried for 24 h and vacuum packed in plastic bags until further handling. Before analysis, freeze-dried HME samples were ground into powder using an agate mortar and pestle set (Z409103-1EA, Sigma Aldrich, Merck Group, St Louis, MO, USA).

2.3.2. Spectral acquisition

Attenuated total reflectance FTIR spectra of freeze-dried samples were acquired in the mid-infrared region (400–4000 cm^{-1}) with a spectrometer (ABB Bomen MB100, ABB Bomem Inc., Quebec, Canada) equipped with a 3-bounce diamond Attenuated Total Reflectance (ATR) unit (DuraScope Dicomp, SensIR Technologies, Danbury, CT, USA) and purged with dried air to reduce the effect of water vapor. Spectra were recorded as the average of 64 scans at 4 cm^{-1} resolution. In order to explore the effect of sample preparation, spectra of intact HME samples (before freeze-drying) were also acquired following the same procedure. All samples were analyzed in duplicate and at room temperature (18 ± 2 °C).

2.3.3. Amide I band spectral deconvolution analysis

To perform the Amide I band spectral deconvolution analysis, first, a band narrowing of the Amide I band of the acquired spectra was carried out applying the second derivative (SD) and Fourier Self-Deconvolution (FSD) methods to find hidden peaks, which were assigned to their corresponding protein secondary structure. These peaks were then fitted to the original spectral profile to calculate their relative area, as shown in Fig. 1 and further described below.

2.3.3.1. Band narrowing and secondary protein structure assignment. Acquired FTIR spectra were truncated from approximately 1600 cm^{-1} to 1700 cm^{-1}, the range corresponding to the Amide I band [29], resulting in 54 data point spectra. A straight baseline was applied by subtracting a straight line passing through the ordinates at 1600 cm^{-1} to 1700 cm^{-1} using Peak analyzer in Origin Pro software, Version 2020 (OriginLab Corporation, Northampton, MA, USA). Although different approaches to baseline correction can be applied—such as performing linear correction in other spectral regions and extending it to the whole spectrum, or using vector normalization with the Amide II band as a reference—many publications do not describe this step in detail [24]. In this work, a straight baseline correction was adopted due to its common use in the literature [15,30–33], with the aim of reflecting practices frequently employed by researchers in the field.

Second derivative (SD) and Fourier self-deconvolution (FSD) were applied and compared as band-narrowing mathematical methods to determine the centre position of hidden peaks under the broad Amide I band. Consistency of the two methods was compared. SD was calculated using Peak Analyzer applying 5-, 7-, and 9-point Savitzky-Golay polynomial filtering to evaluate the effect of the filter's window size on the number and position of the obtained local minima, where changes in the slope can be attributed to the presence of overlapping peaks and shoulders [23]. FSD was performed using Origin's Fourier Self-Deconvolution App, which uses the Kauppinen algorithm to enhance the spectral resolution by dividing the recorded signal in the time domain by the Fourier transform of a Lorentzian line shape function [34]. Values for Gamma (γ) and the smoothing factor (SF) can be selected by the user, where γ is the Lorentzian Full Width at Half Maximum (FWHM) by which the original spectrum is deconvolved, while the SF (a value between 0 and 1) corresponds to a smoothing window function to reduce noise. Different γ (between 10 and 30) and SF (0.1 and 0.15) values were tested. Preliminary analyses showed that SF $>$ 0.15 resulted in unrealistic deconvolution (results not shown) when evaluating centre positions and number of peaks.

As peaks found across different samples were not always consistent, the most repeated nearby central positions (present in 50% or more samples) found by each enhancement method were selected as potential peak centers. Their mean and standard deviation were calculated and assigned to a secondary protein structure according to HMEP-specific literature collected by Bondu et al. [24].

2.3.3.2. Peak fitting and relative area calculation. Non-linear fitting of peaks centred at positions found by SD or FSD was performed on the Amide I region (1600 to 1700 cm^{-1}) of ATR-FTIR spectra of all samples using MATLAB R2011b (MathWorks, MA, USA) and inhouse routines based on the Levenberg–Marquardt algorithm [35,36]. The Gaussian

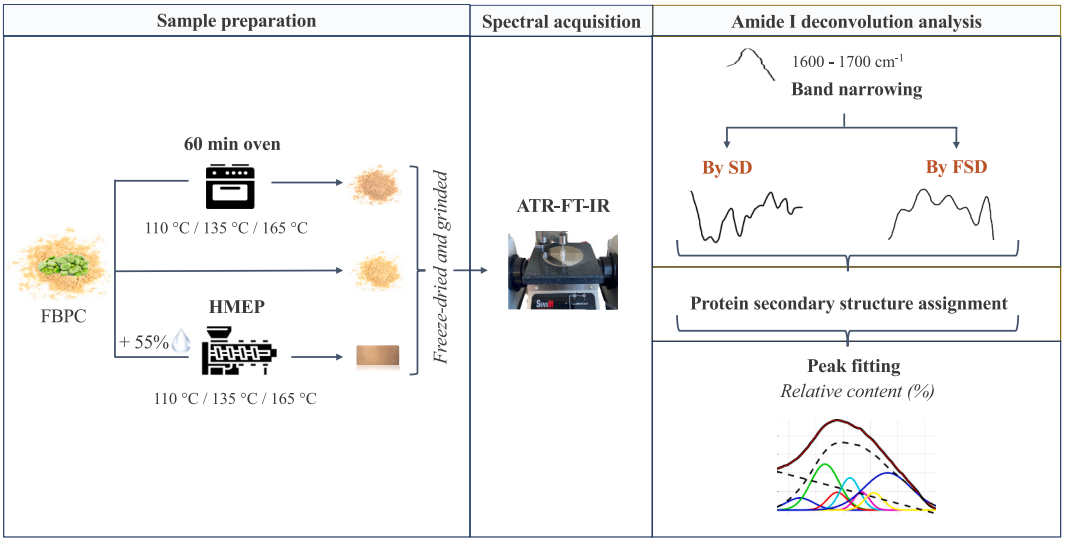

Fig. 1. Experimental procedure for sample preparation, ATR-FTIR spectral acquisition and deconvolution analysis. FBPC: Fava bean protein concentrate; HMEP: High moisture extrusion processing; ATR-FTIR: Attenuated total reflectance Fourier-Transform Infrared spectroscopy; SD: second derivative; FSD: Fourier-Self Deconvolution.

distribution function was applied to describe each of the N identified peaks under the broad Amide I band, where is A the height (i.e. area), μ the centre position, σ the bandwidth, and x the spectral window segment:

$$y_n(x) = \frac{A_n}{\sigma_n \cdot \sqrt{2\pi}} \bullet e^{-\frac{1}{2}\left(\frac{x-\mu_n}{\sigma_n}\right)^2} \quad (1)$$

Additionally, a first-order polynomial was used to compensate for baseline offset (a) and slope (b), and was fitted simultaneously with the other model parameters:

$$y_b(x) = a + b \bullet x \quad (2)$$

The minimization optimized in the non-linear least squares thus becomes the difference between the observed spectrum (per sample) and the following approximation y:

$$y(x) = y_b(x) + \sum_1^N y_n(x) \quad (3)$$

It should be noted here that N and the centre positions μ are determined by the deconvolution scenario (SD or FSD), while A (areas), σ (widths) and the baseline parameters are determined by a second algorithmic optimization step. Fig. 2 shows a graphic example of the fitting for peaks centred at the positions resolved after application of a 7-point SG SD deconvolution procedure, carried out by the inhouse routine on the Amide I region of a raw FBPC sample. It shows the spectrum and overall fit, the base line and the fit-minus-baseline, and eight FTIR bands (minus the estimated baseline).

Once the peaks were fitted, the relative area (%) of the identified peaks (which correspond to the relative content of the assigned protein secondary structures) was calculated by dividing the area count A_n of each individual peak by the total area sum.

2.4. Physicochemical and visual evaluation of HME texture

2.4.1. Instrumental texture analysis

Textural properties were measured using a TA.HD plus C texture analyzer (Stable Micro Systems Ltd., UK) using a 5 kg mass load cell. HME samples were manually cut into 4 × 19 × 19 mm strips (H x W x L) and were tempered at 22 ± 2 °C for at least 2 h before the analysis. Data was acquired and treated using the 6.1.16.0 version of Exponent Stable Micro Systems software (Stable Micro Systems Ltd., UK). Samples were subjected to shear test using a Warner-Bratzler Blade Set with a rectangular slot blade, at a probe speed of 2 mm•s^{-1}. Samples were cut both in the parallel (longitudinal) and perpendicular (transversal) direction to the extrusion flow, to register the maximum longitudinal (F_L) and transversal (F_T) shear force, respectively. Six measurements were performed for each sample. Anisotropy index (AI) was calculated from the ratio between F_L and F_T as an approach to characterize texturization of HME. According to Osen et al. [37], equal values for both shear forces indicate uniform texture with low material anisotropy and without fibrous structure. Therefore, AI values higher than 1 indicated higher anisotropy and presence of fibrous structures in the direction of the extrusion flow.

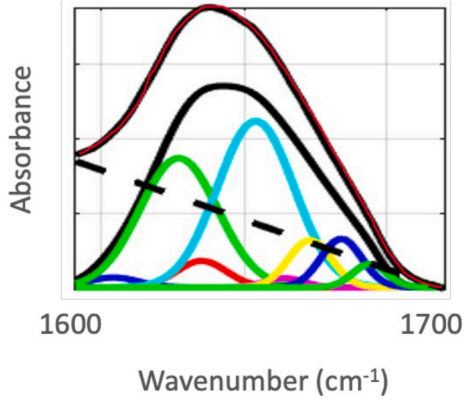

Fig. 2. Example of the Amide I band ATR – FTIR spectrum of a raw FBPC sample and the corresponding fitting of $N = 8$ component peaks found by the 7-point SG SD minus the estimated straight baseline.

2.4.2. Visual evaluation of HME texture

Texturization of HME was evaluated visually by manually folding the samples along their longitudinal axis (parallel to the extrusion flow) to visualise the presence or absence of a characteristic V-shape pattern, which is more pronounced in more textured HME [38]. Pictures of the longitudinal fold of HME samples were taken using a binocular stereo-zoom microscope (SZM-1, OPTIKA Microscopes, Ponteranica, BG, Italy) with 7× magnification and an iPhone SE 2020 camera with 12 MP resolution (Apple Inc., Cupertino, CA, United States).

2.5. Statistical analysis

Secondary protein structure and physicochemical results were analyzed using XLSTAT v2020.1 software (Addinsoft, Paris, France). For secondary protein structure content results, ANOVA was used to evaluate the effect of treatment (Oven or HMEP), temperature, and their interaction. As temperature and the interaction temperature*treatment had no significant effect on protein structure (data not shown), one-way ANOVA including only the effect of treatment (Oven or HMEP) was carried out, including Raw FBPC for comparison purposes. One-way ANOVA was carried out to assess the effect of HMEP temperature on physiochemical and AI of HME. All mean values were compared by the Tukey HSD test ($p < 0.05$).

3. Results and discussion

3.1. Effect of ATR-FTIR analysis procedure on the determination of FBPC and HME secondary protein structures

3.1.1. Effect of sample preparation

Fig. 3 shows the normalized spectra of the Amide I band shape (between 1600 and 1700 cm^{-1}) of deionized water, of a HME sample produced at 110 °C before water removal (intact) and after its elimination by freeze-drying. As can be seen in this figure, the spectrum of the intact HME sample (dashed line in Fig. 3) presents a sharper profile centred at around 1637 cm^{-1} compared to that of the freeze-dried sample (dotted line in Fig. 3), which presents a wider centre around 1645 cm^{-1}. This shift can be related to the water present in the intact HME sample. The spectrum of water (continuous line in Fig. 3) clearly shows a peak at 1635 cm^{-1}, which is caused by O-H-O scissors-bending [39] and interferes with the Amide I band. Therefore, water should be eliminated before extracting any protein-related information from the Amide I band. Freeze-drying is the most established procedure used to remove water from the spectra for Amide band deconvolution. However, the dehydration treatment can induce conformational changes—specifically an increase in the α-helical and β structure fractions [40,41]—which could influence protein structure quantification. Still, compared to different drying methods, freeze-drying causes less protein denaturation [42] and can help preserve more disordered structures present in the native sample [40]. There are alternative procedures that can be carried out to overcome the effect of water on the Amide I band such as substitution of water by deuterium oxide (D_2O) in the sample, which has been extensively used in protein structure studies. However, its use might be too expensive in the specific case of HMEP research [24]. Another alternative procedure is the mathematical subtraction of the reference spectrum of pure water from the sample's spectrum. This may however not be fully adequate as the interaction of protein with

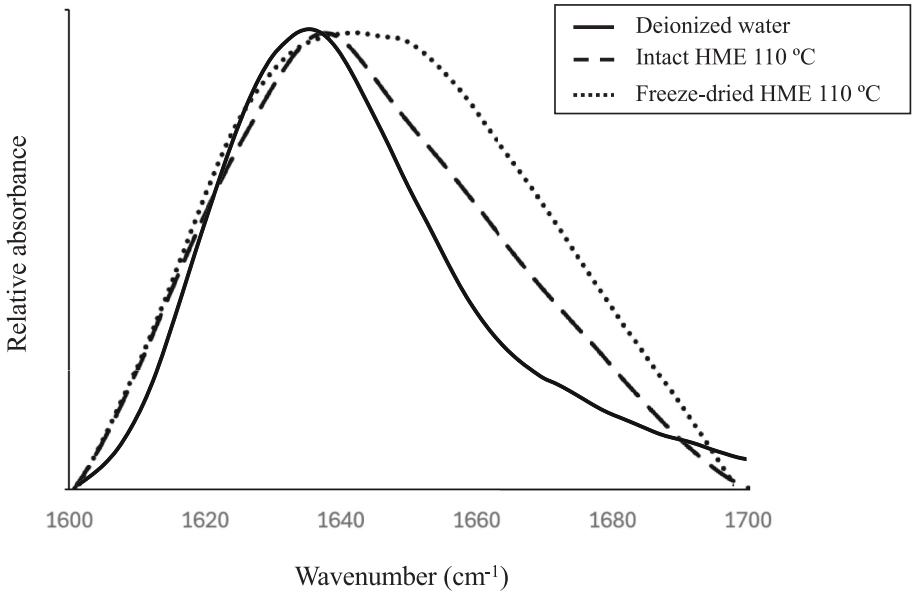

Fig. 3. Amide I band region (1600–1700 cm^{-1}) of deionized water (continuous line), intact (dashed line) and freeze-dried (dotted line) HME samples produced at 110 °C, after normalization and baseline correction.

water in the sample can change the shape of the H_2O band. Besides, selection of the right scaling factor applied to the water spectrum to be subtracted can be challenging, and the subtraction of a very strong water band leads to a decrease of the effective signal-to-noise ratio [43]. Overall, freeze-drying can be considered a good compromise in terms of processing time, resources, and effect on protein denaturation and could explain why most authors working with HMEP choose to freeze-dry the sample before secondary protein structure analysis using FTIR [24].

3.1.2. *Effect of band-narrowing procedure for hidden peak finding*

Table 1 shows the most repeated peak centre positions found by each mathematical procedure used (SD or FSD) and the corresponding possible secondary structure assignment according to the ranges gathered by Bondu et al. [24] from a collection of HMEP-specific publications. Features that were not highly concurrent across replicate samples were discarded, as they might arise from noise [44]. During calculation of the SD, increasing the window size of the SG smoothing filter resulted

Table 1
Mean peak centre positions (cm^{-1}) ± standard deviation of all samples (n = 34) found by second derivative (SD—after applying 5-, 7- and 9-point Savitzky Golay window size) and Fourier self-deconvolution (FSD—applying different Gamma (γ) values and Smoothing Filters (SF)). *Possible secondary structure assignment based on fava bean-specific reported peaks [47] and peaks reported in HMEP-specific publications gathered by Bondu et al. [24] is indicated for each peak centre position.

Band- narrowing method	Settings	Peak centre positions (cm^{-1}) ± standard deviation									
Second derivative (SD)	5-point SG_{WS}	1604 ± 2.3	1616 ± 1.8	1626 ± 1.4	1636 ± 1.3	1645 ± 1.1	1653 ± 1.0	1662 ± 1.3	1675 ± 1.5	1684 ± 1.4	1694 ± 1.6
	7-point SG_{WS}	1606 ± 1.9	–	1627 ± 1.2	1635 ± 1.7	–	1654 ± 2.4	1664 ± 1.1	1673 ± 1.4	1684 ± 1.3	1693 ± 1.7
	9-point SG_{WS}	–	–	1629 ± 1.7	–	–	1653 ± 1.7	–	–	1689 ± 2.9	–
Fourier self-deconvolution (FSD)	γ = 10; SF: 0.10	–	–	–	1636 ± 1.3	1646 ± 2.2	1652 ± 0.7	–	–	–	–
	γ = 10; SF: 0.15	–	–	–	1637 ± 1.5	1647 ± 1.6	–	–	–	–	–
	γ = 15; SF: 0.10	1607 ± 0.7	–	1627 ± 1.1	1635 ± 1.7	1645 ± 1.9	1653 ± 1.3	1663 ± 1.0	1673 ± 1.0	1684 ± 0.8	1694 ± 1.0
	γ = 15; SF: 0.15	–	–	–	1636 ± 3.8	1649 ± 1.3	–	–	–	–	–
	γ = 20; SF: 0.10	1605 ± 1.2	1616 ± 1.3	1627 ± 2.2	1636 ± 1.7	1645 ± 1.4	1654 ± 1.1	1663 ± 1.1	1673 ± 1.4	1684 ± 1.6	1695 ± 0.0
	γ = 20; SF: 0.15	–	–	–	1633 ± 4.7	–	1651 ± 1.7	–	–	–	–
	γ = 25; SF: 0.10	1605 ± 1.2	1615 ± 1.4	1625 ± 1.4	1636 ± 1.5	1645 ± 1.6	1654 ± 1.2	1663 ± 1.1	1673 ± 1.0	1685 ± 1.8	1696 ± 1.1
	γ = 25; SF: 0.15	1610 ± 1.1	–	1629 ± 2.0	1635 ± 0.9	–	1652 ± 1.8	–	–	–	1691 ± 0.7
	γ = 30; SF: 0.10	1605 ± 1.2	1615 ± 1.4	1625 ± 1.4	1636 ± 1.5	1645 ± 1.6	1654 ± 1.2	1663 ± 1.1	1673 ± 1.0	1685 ± 1.8	1696 ± 1.1
	γ = 30; SF: 0.15	1608 ± 0.7	–	1627 ± 2.4	1635 ± 2.1	–	1652 ± 2.1	1665 ± 1.8	1677 ± 1.7	–	1692 ± 1.1
Secondary structure attribution*		**RC / β / Inter-β**	**β / Inter-β / Anti-β / A**	**β / Inter-β / Intra-β**	**β / Intra-β**	**RC**	**α-helix**	**β-turn**	**β-turn / β**	**β / β-turn / Anti-β**	**β / β-turn / Anti-β / A**

SG_{WS}: Savitzky-Golay filter window size; RC: random coil; β: β-sheet; Inter-β: intermolecular β-sheet; Intra-β: intramolecular β-sheet; Anti-β: anti-parallel β-sheet; A: aggregates.

in a reduced number of peaks found: the 5-point SG filter resolved 10 peaks whereas 7-point and 9-point resolved 8 and 3 peaks, respectively. As previously discussed, SD calculation is especially sensitive to noise in the original spectrum [21], which can give rise to false peaks. That is why peak differentiation is often performed using preprocessing strategies such as the use of SG filters or smoothing procedures to avoid introducing noise amplification [45]. Nevertheless, smoothing of the data often attenuates sharp peaks and could result in an underestimation of the magnitude of the derivative and thus the number of (true) species in the Amide I band [46]. Therefore, as observed in the present results and according to literature [26], smoothing filter selection is clearly a key factor in this kind of analysis, as it needs to remove as much high frequency noise as possible without significantly altering the underlying spectral structure.

In the case of FSD, at a same value of γ, an increase of SF from 0.1 to 0.15, drastically reduced the number of peaks found in all scenarios. On the other hand, at a same SF = 0.1, an increase of γ from 10 to 15, and up to 20, suggested a larger number of peaks (3, 9, and 10, respectively). However, further increase of γ from 20 to 25/30 when SF = 0.1, did not result in an additional number of peaks. Similarly, when SF was set at 0.15, an increase in γ eventually resolved a major number of peaks. Finding the right combination of these two parameters is a crucial step, as excessive filtering can cause under-estimation (not allowing to identify all real peaks) while excessive band narrowing can lead to over-estimation (e.g. mistakenly identifying noise as peaks or resulting in large negative side-lobes [34]). However, this selection is not straightforward. According to Lórenz-Fonfría et al. [44], it is only when the band width of the input broadening function (determined by γ) matches the actual broadening function of the bands, that peaks for further strict self-deconvolution can be achieved. However, this is only possible for spectra made of bands of identical and known width, which is rarely the case as spectra often contain bands of different and unknown appearance [48]. In such circumstances, most of the bands will be either under-deconvoluted or over-deconvoluted [48], meaning that too little or an excessive number of peaks will be resolved, respectively. This issue causes FSD to be user-dependent, meaning that choices made during the process can affect the results and thus the chemical interpretation.

Table 1 shows that although the number of features found varied for the different filter thresholds, most peaks found by the different SD setups matched with those found in different scenarios of FSD. In addition to the different number of identified peaks (discussed above), a shift in peak centre positions was also observed across different parameter selection scenarios in both SD and FSD. Regarding SD, after applying a 9-point SG smoothing filter, the peak at 1684 cm^{-1} shifted to 1689 cm^{-1} while the peak at 1693 cm^{-1} was no longer identified. Similarly, for FSD, some of the peak centre positions found when applying SF = 0.1 were either no longer identified or shifted (e.g. for γ = 15, the peak centred at 1645 cm^{-1} shifted to 1649 cm^{-1}, while the peak at 1653 cm^{-1} disappeared after applying SF = 0.15). These changes could be indicative of excessive smoothing, manifesting as shifts in the overlapped peak centres or merger of adjacent peaks into broader bands [26]. All this can lead to significant loss in spectral profile information and misinterpretation of the results.

Since both band-narrowing procedures are sensitive and can easily introduce distortions, it is recommended that spectra are subjected to both SD and FSD and only features identified by both should be considered for secondary structure assignment [21]. This approach should allow a more robust identification of real features (present in both derivative and deconvolved spectra) and detection of artifacts (most probably different for both SD and FSD). However, the obtained results demonstrate that not only the band-narrowing procedure used but also the settings used within each procedure are relevant for protein secondary structure analysis. In this sense, the use and comparison of different settings would also be recommended to evaluate possible differences in the obtained results and select the most adequate for further peak fitting.

In this paper, peak centre positions found by SD after 5-point ($N = 10$ components) and 7-point SG filtering ($N = 8$ components) matched with positions found by FSD using $\gamma = 20$, $\gamma = 25$ and $\gamma = 30$ with SF = 0.1 (allowing a deviation of maximum 2 cm^{-1}). Therefore, these peak centres were chosen to be used for further peak fitting.

3.1.3. Effect of SD band-narrowing procedure on secondary protein structure analysis of thermally and HMEP treated FBPC

According to the results obtained in section 3.1.2, spectra obtained from each of the samples were processed using a SD band narrowing procedure with 5-point and 7-point SG window filter to study the effect of different treatments (Oven temperature treatment and HMEP), different temperatures within each treatment (110 °C, 135 °C and 165 °C), and their interaction (treatment*temperature). Only the treatment significantly influenced the relative content of secondary protein structures ($p < 0.05$), while temperature and the interaction treatment*temperature showed no significant effect ($p > 0.05$; results not shown). For this reason, for each of the different SD settings only the effect of the treatment applied on secondary protein structure was evaluated, including Raw FBPC for comparison purposes. The relative area of each peak fitted to the Amide I band (or relative content of the

Table 2
Mean relative content (%) (± standard deviation, $n = 6$) of secondary protein structures of FBPC after different processing treatments (Raw, oven, HMEP) using peaks obtained after SD using 5-point and 7-point Savitzky-Golay smoothing filter.[a-b]

SD settings	Peak position (cm^{-1})	Secondary protein structure assigned	FBPC processing treatments		
			Raw	Oven	HMEP
5-point	1604	(RC / β / Inter-β)	3.3 ± 0.84	4.0 ± 0.31	4.57 ± 0.80
	1616	(β / Inter-β / Anti-β / A)	8.9 ± 0.28[b]	8.8 ± 0.21[b]	10.1 ± 0.58[a]
	1626	(β / Inter-β / Intra-β)	11.4 ± 0.47	12.6 ± 0.47	12.6 ± 0.41
	1636	(β / Intra-β)	17.3 ± 0.43	17.2 ± 0.36	16.2 ± 0.57
	1645	(RC)	10.72 ± 0.45	10.9 ± 0.28	11.0 ± 0.35
	1653	(α-helix)	9.7 ± 0.94	10.2 ± 0.34	10.5 ± 1.05
	1662	(β-turn)	17.0 ± 1.48	15.2 ± 0.64	14.6 ± 2.75
	1675	(β / β-turn)	14.3 ± 2.60	15.9 ± 1.18	15.32 ± 3.43
	1684	(β / β-turn / Anti-β)	5.7 ± 4.29[a]	2.7 ± 0.57[b]	2.2 ± 1.44[b]
	1694	(β / β-turn / Anti-β / A)	1.9 ± 1.19[b]	2.5 ± 0.41[b]	3.1 ± 0.35[a]
	Goodness of fit (R^2)*		***>0.999***	***>0.999***	***>0.998***
7-point	1604	(RC / β / Inter-β)	0.9 ± 1.14[b]	1.8 ± 0.40[ab]	2.2 ± 0.6[a]
	1626	(β / Inter-β / Intra-β)	35.0 ± 1.56[b]	35.1 ± 1.17[b]	38.7 ± 1.34[a]
	1635	(β / Intra-β)	6.2 ± 2.52[a]	2.9 ± 0.83[b]	2.93 ± 0.85[b]
	1654	(α-helix/RC)	38.0 ± 6.65[b]	44.6 ± 2.10[a]	38.7 ± 1.68[b]
	1664	(β-turn)	2.0 ± 1.20[a]	0.9 ± 0.32[b]	0.9 ± 0.39[b]
	1673	(β / β-turn)	5.8 ± 1.41[b]	5.7 ± 0.61[b]	7.7 ± 0.78[a]
	1684	(β / β-turn / Anti-β)	10.3 ± 5.11[a]	6.3 ± 0.51[b]	5.9 ± 0.47[b]
	1694	(β / β-turn / Anti-β / A)	1.8 ± 1.17[b]	2.9 ± 0.42[a]	3.0 ± 0.35[a]
	Goodness of fit (R^2)*		***>0.999***	***>0.999***	***>0.998***

[a-b] Different letters within the same row indicate significant differences between FBPC processing treatments ($p < 0.05$).

* Goodness of fit is presented as the minimum R^2 value of all samples within a processing treatment, for each SD setting.

attributed secondary structures), determined by 5-point and 7-point SG SD, for each FBPC treatment (Raw, Oven and HMEP) is shown in Table 2.

When using 5-point SG SD, except for the more extreme peaks (centred at 1604 cm^{-1}, 1684 cm^{-1}, and 1694 cm^{-1}), which presented lower relative areas, all peaks presented values between 8% and 20%. For many of the peaks resolved by this procedure, no significant changes were detected across different treatments. Still, a significant increase of the relative area for the peaks centred at 1616 cm^{-1} and 1694 cm^{-1} ($p < 0.05$) in HME samples was observed in comparison to raw FBPC and FBPC thermally treated in the oven. This could correspond to an increase in β-sheet, intermolecular β-sheet, anti-parallel β-sheet, β-turn and/or protein aggregates. At the same time, a significant decrease on the relative area of the peak located at 1684 cm^{-1} of both oven (2.7%) and HMEP (2.2%) treatments in comparison to raw FBPC (5.7%) was observed ($p < 0.05$), which can be related to a decrease in other β structures (possibly β-sheet, β-turn, or antiparallel β-sheet).

However, when fitting the reduced number of peaks identified applying 7-point SG SD, different results were observed. In general, samples presented higher relative areas for peaks located at 1626 cm^{-1} (35–39%) and 1654 cm^{-1} (38–45%), potentially corresponding to different β-sheet and to α-helix forms, respectively. Other studies have also shown that β-sheet is a predominant secondary protein structure in legumes, however, they have suggested lower proportions of α-helix [7,49,50]. It is known that an overlapping of α-helix with random coil occurs in the range of 1640–1660 cm^{-1}, which might also interfere with β-turn peak structures (1665 and 1660 cm^{-1}) [51]. Therefore, according to attributions reported in literature, random coil regions or β-turn could potentially be contributing to the peak centred at 1654 cm^{-1}, which could explain its higher relative area. Nevertheless, what is often referred to in the spectroscopy literature as random coil corresponds to regions of a protein that lack a stable, well-defined secondary structure. The term 'random coil' actually refers to a statistical distribution [52] where protein conformations are oriented randomly while still being bonded to adjacent structures. Many unfolded proteins in solution or above their melting temperatures assume approximate random coils [53]. Yet, in a real denatured polypeptide chain, interactions between sidechains will bias the system from the random coil distribution toward more compact states or aggregates [54].

Moreover, the results based on the peaks resolved by 7-point SG SD detected more significant differences across samples compared to 5-point SG SD results. They suggested that HMEP caused a significant increase in the relative area of the peak centred at 1604 cm^{-1}, 1626 cm^{-1}, 1673 cm^{-1}, and 1694 cm^{-1} ($p < 0.05$) which, according to the HMEP-specific publications gathered by Bondu et al. [24], could be attributed to random coil, β-sheet, intermolecular β-sheet, intramolecular β-sheet, antiparallel β-sheet, β-turn, and/or protein aggregates. Results also showed a significant increase of the peak located at 1654 cm^{-1} in FBPC samples that were subjected to oven thermal treatment, and indicated that both oven thermal treatment and HMEP caused a significant decrease in the relative area of the peak located at 1635 cm^{-1}, 1664 cm^{-1} and 1684 cm^{-1}, which could correspond to β-sheet, intramolecular β-sheet, antiparallel β-sheet and/or β-turn.

Overall, the inconsistency in secondary structure quantification obtained using 5- and 7-point SG SD evidences the importance of parameter selection during peak finding for Amide I band deconvolution. The smoothing filter applied influenced the number of contributing features and at the same time had an effect on the peak fitting step, suggesting once again that the accuracy of the results highly depends on the users' decisions throughout the procedure.

3.2. Effect of temperature and HMEP on secondary protein structure

Despite the inconsistencies between SD and FSD in the identification of the contributing features and the challenging protein structure attribution, results shown in Table 2 generally suggested that both dry temperature treatment and HMEP caused a decrease of some β-sheet forms related to the peak centred at 1635 cm^{-1} (potentially assigned to β-sheet, intramolecular β-sheet, and/or antiparallel β-sheet), which could be present initially in FBPC, followed by an increase in other structures.

Interestingly, for dry temperature treatment, an increase of the peak located at 1654 cm^{-1} could potentially be suggesting an increase in α-helix structure. However, α-helix is an ordered structure that is maintained by intramolecular hydrogen bonding [55] which would be expected to decrease during dry heating, as reported by Carbonaro et al. [7] for common bean and chickpea proteins. In addition to a decreasing content of α-helix, high temperature has also been reported to significantly increase the proportion of random coil in quinoa protein isolate [56]. Since α-helix overlaps with random coil in the range of 1640–1660 cm^{-1}, as previously discussed, the increase in the relative area at 1654 cm^{-1} could potentially be indicating that oven treatment caused an increase in random coil—or aggregates—in FBPC.

On the other hand, HMEP caused an increase of other β forms including intermolecular β-sheet and/or aggregates which usually appear at lower frequency band positions and involve new intermolecular interactions [57], related to the peaks located at 1604 cm^{-1}, 1616 cm^{-1} and 1626 cm^{-1}. These new interactions could be forming after unfolding of β-sheet structures by disruption of intramolecular and strong intermolecular bonds, followed by new intermolecular bond creation during HMEP, as reported by other authors [58]. Nevertheless, the fact that no significant differences were observed between HME samples produced at different temperatures suggested that, within the range of extrusion temperatures studied, the effect of HMEP on protein secondary structure of FBPC was most probably due to the combination of temperature, pressure and shear force applied during the process. All of these could be causing proteins to unfold and rearrange into the final HME, without a significant effect of increased extrusion temperatures in the studied range.

Moreover, the results also suggested a potential change in β-turns due to temperature treatment and to HMEP. However, it is difficult to draw conclusions on the effect of temperature treatments and HMEP on this structure as it could be assigned to several peaks with opposite tendencies (increasing area of peaks at 1673 cm^{-1} and 1694 cm^{-1} whereas decreasing areas at 1664 cm^{-1} and 1684 cm^{-1}). At the same time, all these peaks have been assigned to different structures (not only to β-turn) throughout different works, adding difficulty to the interpretation. It is essential to notice that β-turn analysis is complex due to various reasons including their overlap with other structures, the potential absence of a stabilizing hydrogen bond, and the numerous types of β-turns [59]. In this regard, contrasting results have been reported in literature in relation to changes in β-turn caused during HMEP. For instance, Mao et al. [58] and Wang et al. [60] found that HMEP caused a decrease in β-turn in rice protein, in soy protein and in wheat mixtures. Contrarily, other works have reported that HMEP can bond unfolded structures into new ones including β-turns [61]. In addition, Beck et al. [62] proposed that formation of intermolecular aggregates in pea protein isolates could be made of β-turn structures or antiparallel β-sheet, which increased during heat treatment and shear force application. Yet, it is worth mentioning that the ability of FTIR to distinguish different types of β-sheet including anti-parallel arrangements is debated [63].

Overall, although the accuracy of FTIR analysis of the Amide I region is constrained by its procedural setup, a general understanding of protein secondary structure changes induced by temperature treatment and HMEP has been obtained. It should be emphasized, however, that this technique is not adequate for quantitative purposes. The frequent lack of details reported regarding these steps [24] makes comparison between studies and reproducibility quite challenging. For this reason, future studies should, at a minimum, provide transparent reporting of the analytical procedures employed—including baseline correction and deconvolution analysis—and exercise greater caution in drawing conclusions. These limitations become even more pronounced in complex

protein mixtures such as those investigated in this paper. Therefore, it is important to highlight the specific constraints of FTIR-based quantification in order to encourage careful interpretation of results in future applications. Furthermore, attention should be directed toward investigating additional analytical steps that may influence the technique, such as baseline correction procedures. Despite in this paper straight baseline correction from 1600 cm^{-1} to 1700 cm^{-1} was applied for comparison with published works, Amide I band is not isolated from adjacent peaks in the IR spectrum. Therefore, future studies should investigate the use of broader spectral baseline methods to better account for these contributions. Moreover, it is worth noting that, although deconvolution can serve as an exploratory tool for identifying broad structural motifs, it does not explicitly account for nearest-neighbour coupling arising from through-bond effects [64]. This limitation further underscores that its quantitative reliability is restricted when compared with more advanced analytical approaches. In this context, several authors have proposed improved procedures to increase reliability and objectivity of Amide I deconvolution [26,40,65].

As an additional challenge, changes on secondary protein structures during HMEP can also be influenced by the protein source [58], the protein extraction method [66] and other possible treatments of the protein ingredient such as defatting [67] that may affect protein structure prior to HMEP.

As a future perspective, alternative multivariate analytical methods—such as factor analysis, singular value decomposition, or multiple neural network [65]—could be employed and compared with the deconvolution techniques based on FSD or second derivative analysis as possible alternatives to separate the overlapping signals in the amide bands. Moreover, the application of complementary spectroscopic techniques—such as Raman spectroscopy or circular dichroism [68]—could provide supporting evidence to either reinforce or question the findings derived from Amide I band deconvolution, advancing the methodological standardization of spectroscopic determination of protein secondary protein structure. This, tailored to specific case studies, could allow a more precise quantification of protein secondary structure, ultimately contributing to a deeper understanding of protein extrusion and its further implications, such as its relation with protein digestibility and nutritional value [69–71].

3.3. Effect of HMEP temperature on FBPC texturization and relationship with secondary protein structure

Table 3 shows the effect of extrusion temperature on the anisotropy index (AI) of HME. HME processed at 110 °C and 135 °C showed AI values close to 1 (0.9 and 1.0, respectively), indicating low material anisotropy and absence of fibrous structures [37]. However, significantly higher values were observed for HME extruded at 165 °C (1.3; $p < 0.05$), revealing that higher extrusion temperatures enhance the formation of fibrous structures in the direction of the extrusion flow (AI >1). Similar results were observed during visual evaluation, for which HME processed at 110 °C and 135 °C showed hardly or no V-shape, while HME produced at 165 °C did show a V-shape profile in the direction of the extrusion flow (marked in blue in Fig. 4) indicating material texturisation. In addition, fibrous structures were also observed between the two splits resulting from the longitudinal folding for HME obtained at 165 °C (indicated with a red arrow in Fig. 4). Despite there being many (interacting) parameters affecting protein texturization during HMEP [72], our results evidence the effect of increased extrusion temperature on protein texturization. However, at the same time, no significant variation in protein conformation was observed between HME produced at different temperatures (as discussed in Section 3.2). Although the formation of a new three-dimensional network requires globular proteins—especially those from leguminous sources—to unfold and realign [73], and although high temperature, pressure, and shear forces during HMEP induced changes in protein secondary structure, the resulting anisotropic states observed in the HME products could not be directly linked to differences in protein conformation by means of FTIR Amide I band deconvolution. Despite variations in extrusion temperature could be expected to cause different level of protein modifications, structural modifications continue during the cooling stage—where proteins undergo realignment—which may reduce the observable differences in the final HME. Instead, the increased anisotropy of HME obtained at increased HMEP temperature could be related to the effect of temperature on the viscosity of the melt and the flow characteristics, which play an important role on the morphology development of plant-based HME [74] and may induce the formation of layered structures by phase separation in the cooling die under the influence of a temperature gradient [75].

Table 3
Mean anisotropy index (± standard deviation) of HME produced at different extrusion temperatures.

HMEP temperature [°C]	Anisotropy index [−]
110	0.9 ± 0.06^{b}
135	1.0 ± 0.03^{b}
165	1.3 ± 0.26^{a}

a,b different letters indicate significant differences ($p < 0.05$).

Nevertheless, texturisation can also be influenced by distribution and stabilisation of proteins and other components including water [74], polysaccharides [76] and lipids [77] present in the HME. In this regard, raw material characteristics do play an important role in the processing of HME and may influence protein conformation. For example, Zhang et al. [78] reported that the addition of exogenous polysaccharides to peanut protein promoted protein conformational changes and, at the same time, influenced the fibrous structure formation. Similarly, Guerrero et al. [79] highlighted the usefulness of employing FTIR to assess changes in the structure of proteins and interactions that have taken place between biopolymers used in blends during low moisture extrusion processing (LMEP) and to explain physical properties of extrudates. Moreover, Jiang et al. [10] also showed the potential of mixing protein sources to obtain blends with different protein structures with the aim of improving textural properties of extrudates.

This suggests that, despite it not being able to explain the different anisotropic characters of FBPC HME produced at different temperatures based on protein structural changes within the studied range, FTIR could be useful to study further implications of molecular conformation from different raw material blends to be texturised by HMEP. Additionally, further research the influence of other HMEP parameters—such as feeding rates, screw speed, etc.—on protein structure and anisotropy could provide deeper insights into the implications of structural changes on HME texturisation.

4. Conclusions

FTIR Amide I band deconvolution is a useful tool to evaluate protein secondary structure changes at an exploratory level. However, due to its high sensitivity, factors such as sample preparation and the analysis procedure (including the band-narrowing method, the selection of smoothing filters, and peak secondary structure attribution) should be designed carefully and systematically to avoid unpredictable or unjustified variations in quantitative outcomes. Despite the inherent challenges of FTIR analysis, indications of a changing trend in the secondary structure of FBPC following HMEP were observed. However, this could not explain the different anisotropic character of HME from FBPC processed at different temperatures within the studied range and conditions used. Looking ahead, careful and well-documented use of FTIR Amide I band deconvolution could strengthen confidence in this technique and support a deeper understanding of protein extrusion and its further implications in relation to HMEP.

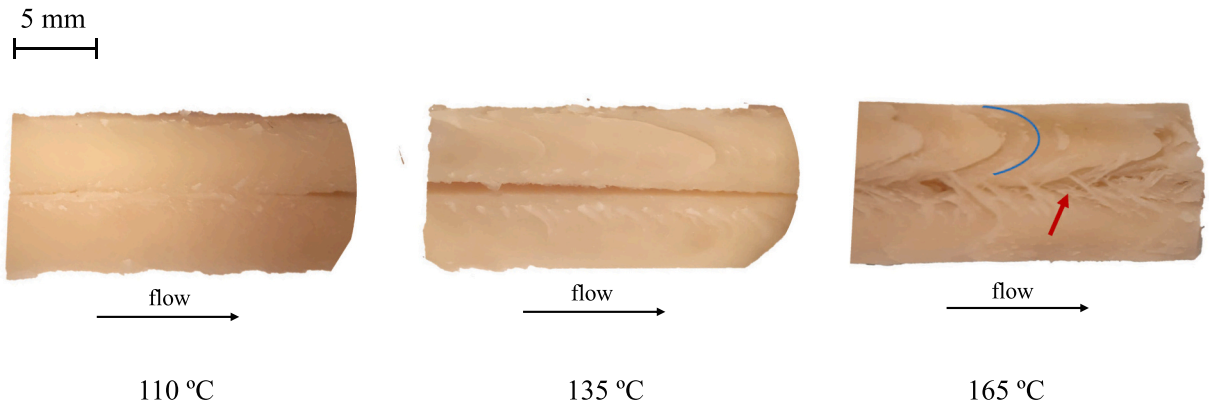

Fig. 4. Images of longitudinally folded HME samples processed at different temperatures (110 °C, 135 °C and 165 °C). The **blue arc** indicates the presence of V-shape and the fibrous structures joining the two longitudinal splits are indicated with a **red arrow**. (For interpretation of the references to colour in this figure legend, the reader is referred to the web version of this article.)

Declaration of competing interest

The authors declare that they have no known competing financial interests or personal relationships that could have appeared to influence the work reported in this paper.

Acknowledgements

This work was supported by the SENSANALOG project funded by MICIU/AEI/10.13039/501100011033 and ERDF/EU [PID2021-122285OR-I00], and by the CROPDIVA project funded by the European Union's Horizon 2020 research and innovation programme [Grant Agreement 101000847]. C. Barnés-Calle gratefully acknowledges receiving a predoctoral fellowship [FPU20/04009] from the Spanish MCIN/AEI/10.13039/501100011033 and "ESF Investing in your Future", and a mobility grant from the Institute of Agrifood Research and Technology (IRTA) within the Incentives for Research Program 2023. Acknowledgements are extended to the SensorFINT COST action (CA19145) funded by the European Union for supporting C. Barnés-Calle and E. Fulladosa with mobility grants for Short Term Scientific Missions, to the Consolidated Research Group (TECQUAL 2021 SGR 00461), to the Agència de Gestió d'Ajuts Universitaris i de Recerca (AGAUR), to the CERCA Program of the Generalitat de Catalunya, and to the University of Copenhagen.

Data availability

Data will be made available on request.

References

[1] Good Food Institute, Plant protein primer. https://gfi.org/wp-content/uploads/2021/02/2021-02-23_Plant_Protein_Primer_GFI.pdf, 2021.
[2] S. Multari, D. Stewart, W.R. Russell, Potential of fava bean as future protein supply to partially replace meat intake in the human diet, Compr. Rev. Food Sci. Food Saf. 14 (5) (2015) 511–522, https://doi.org/10.1111/1541-4337.12146.
[3] C. Barnés-Calle, G. Matas, P. Gou, E. Fulladosa, Fibre-like structure formation in fava bean protein based extrudates: effects of extrusion inputs and potential of outputs for process control, Future Foods 12 (2025) 100697, https://doi.org/10.1016/j.fufo.2025.100697.
[4] M. Toldrà, D. Parés, C. Barnés-Calle, P. Gou, E. Fulladosa, Techno-functional and physico-chemical properties of high moisture extrudates from faba bean (*Vicia faba*) protein concentrate using different extrusion conditions, LWT (2025) 117898, https://doi.org/10.1016/j.lwt.2025.117898.
[5] M.S. Alam, J. Kaur, H. Khaira, K. Gupta, Extrusion and extruded products: changes in quality attributes as affected by extrusion process parameters: a review, Crit. Rev. Food Sci. Nutr. 56 (3) (2016) 445–473, https://doi.org/10.1080/10408398.2013.779568.
[6] E. Schmid, A. Farahnaky, B. Adhikari, P.J. Torley, High moisture extrusion cooking of meat analogs: a review of mechanisms of protein texturization, Compr. Rev. Food Sci. Food Saf. 21 (6) (2022) 4573–4609, https://doi.org/10.1111/1541-4337.13030.
[7] M. Carbonaro, P. Maselli, A. Nucara, Relationship between digestibility and secondary structure of raw and thermally treated legume proteins: a Fourier transform infrared (FT-IR) spectroscopic study, Amino Acids 43 (2) (2012) 911–921, https://doi.org/10.1007/s00726-011-1151-4.
[8] C. Ma, S. Xia, J. Song, Y. Hou, T. Hao, S. Shen, K. Li, C. Xue, X. Jiang, Yeast protein as a novel dietary protein source: comparison with four common plant proteins in physicochemical properties, Curr. Res. Food Sci. 7 (2023) 100555, https://doi.org/10.1016/j.crfs.2023.100555.
[9] A. Madurapperumage, N. Johnson, P. Thavarajah, L. Tang, D. Thavarajah, Fourier-transform infrared spectroscopy (FTIR) as a high-throughput phenotyping tool for quantifying protein quality in pulse crops, The Plant Phenome J. 5 (1) (2022), https://doi.org/10.1002/ppj2.20047.
[10] W. Jiang, J. Feng, X. Yang, L. Li, Structure of pea protein-based complexes on high-moisture extrusion: raw materials and extrusion zones, LWT 194 (2024) 115823, https://doi.org/10.1016/j.lwt.2024.115823.
[11] D. Sun, B. Zhang, C. Zhou, W. Ren, M. Wu, Effect of high-moisture extrusion process on quality attribute and fibrous formation mechanism of pea protein: insight into dynamic changes of textural protein, Innovative Food Sci. Emerg. Technol. 89 (2023) 103486, https://doi.org/10.1016/j.ifset.2023.103486.
[12] Y. Zhang, G.H. Ryu, Effects of process variables on the physicochemical, textural, and structural properties of an isolated pea protein-based high-moisture meat Analog, Foods 12 (24) (2023) 4413, https://doi.org/10.3390/foods12244413.
[13] S. Krimm, J. Bandekar, Vibrational spectroscopy and conformation of peptides, polypeptides, and proteins, Adv. Protein Chem. 38 (1986) 181–364.
[14] J. Bandekar, Amide modes and protein conformation, Biochim. Biophys. Acta Protein Struct. Mol. Enzymol. 1120 (2) (1992) 123–143, https://doi.org/10.1016/0167-4838(92)90261-b.
[15] H. Yang, S. Yang, J. Kong, A. Dong, S. Yu, Obtaining information about protein secondary structures in aqueous solution using Fourier transform IR spectroscopy, Nat. Protoc. 10 (3) (2015) 382–396, https://doi.org/10.1038/nprot.2015.024.
[16] F. Fanari, G. Carboni, F. Desogus, M. Grosso, M. Wilhelm, A chemometric approach to assess the rheological properties of durum wheat dough by indirect FTIR measurements, Food Bioprocess Technol. 15 (5) (2022) 1040–1054, https://doi.org/10.1007/s11947-022-02799-z.
[17] A. Nawrocka, M. Krekora, Z. Niewiadomski, A. Miś, FTIR studies of gluten matrix dehydration after fibre polysaccharide addition, Food Chem. 252 (2018) 198–206, https://doi.org/10.1016/j.foodchem.2018.01.110.
[18] C. Pérez, K. Griebenow, Fourier-transform infrared spectroscopic investigation of the thermal denaturation of hen egg-white lysozyme dissolved in aqueous buffer and glycerol, Biotechnol. Lett. 22 (23) (2000) 1899–1905, https://doi.org/10.1023/a:1005645810247.
[19] A. Barth, Fine-structure enhancement — assessment of a simple method to resolve overlapping bands in spectra, Spectrochim. Acta A Mol. Biomol. Spectrosc. 56 (6) (2000) 1223–1232, https://doi.org/10.1016/S1386-1425(00)00228-6.
[20] A. Dong, P. Huang, W.S. Caughey, Protein secondary structures in water from second-derivative amide I infrared spectra, Biochemistry 29 (13) (1990) 3303–3308, https://doi.org/10.1021/bi00465a022.
[21] M. Jackson, H.H. Mantsch, The use and misuse of FTIR spectroscopy in the determination of protein structure, Crit. Rev. Biochem. Mol. Biol. 30 (2) (1995) 95–120, https://doi.org/10.3109/10409239509085140.
[22] D.J. Moffan, H.H. Mantsch, Fourier resolution enhancement of infrared spectral data, Methods Enzymol. 210 (1992) 192–200.
[23] A. Sadat, I.J. Joye, Peak fitting applied to Fourier transform infrared and Raman spectroscopic analysis of proteins, Appl. Sci. 10 (17) (2020) 5918, https://doi.org/10.3390/app10175918.
[24] C. Bondu, F. Gimeno, P. Evon, G. Vaca-Medina, A. Rouilly, Use of FTIR to study secondary structure of texturized plant proteins by high moisture extrusion cooking, a comprehensive review, Food Res. Int. 197 (2024) 115147, https://doi.org/10.1016/j.foodres.2024.115147.

[25] D.M. Byler, H. Susi, Examination of the secondary structure of proteins by deconvolved FTIR spectra, Biopolymers 25 (3) (1986) 469–487, https://doi.org/10.1002/bip.360250307.
[26] A.P. Fellows, M.T.L. Casford, P.B. Davies, Spectral analysis and deconvolution of the amide I band of proteins presenting with high-frequency noise and baseline shifts, Appl. Spectrosc. 74 (5) (2020) 597–615, https://doi.org/10.1177/0003702819898536.
[27] W.K. Surewicz, H.H. Mantsch, D. Chapman, Determination of protein secondary structure by Fourier transform infrared spectroscopy: a critical assessment, Biochemistry 32 (2) (1993) 389–394, https://doi.org/10.1021/bi00053a001.
[28] C. Barnés-Calle, G. Matas, A. Claret, L. Guerrero, E. Fulladosa, P. Gou, High moisture extrusion of pea protein isolate to mimic chicken texture: instrumental and sensory insights, Food Hydrocoll. 154 (2024) 110129, https://doi.org/10.1016/j.foodhyd.2024.110129.
[29] J. Sturgis, B. Robert, E. Goormaghtigh, Transmembrane Helix stability: the effect of Helix-Helix interactions studied by Fourier transform infrared spectroscopy, Biophys. J. 74 (2) (1998) 988–994, https://doi.org/10.1016/S0006-3495(98)74022-6.
[30] J.S. Cobb, V. Zai-Rose, J.J. Correia, A.V. Janorkar, FT-IR spectroscopic analysis of the secondary structures present during the desiccation induced aggregation of elastin-like polypeptide on silica, ACS Omega 5 (14) (2020) 8403–8413, https://doi.org/10.1021/acsomega.0c00271.
[31] J. Peng, K. Zhu, X. Guo, H. Zhou, The impact of phosphates on the fibrous structure formation of textured wheat gluten, Food Hydrocoll. 119 (2021) 106844, https://doi.org/10.1016/j.foodhyd.2021.106844.
[32] B. Srour, S. Bruechert, S.L.A. Andrade, P. Hellwig, Secondary structure determination by means of ATR-FTIR spectroscopy, Methods Mol. Biol. 1635 (2017) 195–203, https://doi.org/10.1007/978-1-4939-7151-0_10.
[33] M. Ye, R. Zhou, Y. Shi, H. Chen, Y. Du, Effects of heating on the secondary structure of proteins in milk powders using mid-infrared spectroscopy, J. Dairy Sci. 100 (1) (2016) 89–95, https://doi.org/10.3168/jds.2016-11443.
[34] J.K. Kauppinen, D.J. Moffatt, H.H. Mantsch, D.G. Cameron, Fourier self-deconvolution: a method for resolving intrinsically overlapped bands, Appl. Spectrosc. 35 (3) (1981) 271–276, https://doi.org/10.1366/0003702814732634.
[35] R.H. Barham, W. Drane, An algorithm for least squares estimation of nonlinear parameters when some of the parameters are linear, Technometrics 3 (1972) 757.
[36] D.W. Marquardt, An algorithm for least-squares estimation of nonlinear parameters, J. Soc. Ind. Appl. Math. 11 (2) (1963) 431–441, https://doi.org/10.1137/0111030.
[37] R. Osen, S. Toelstede, F. Wild, P. Eisner, U. Schweiggert-Weisz, High moisture extrusion cooking of pea protein isolates: raw material characteristics, extruder responses, and texture properties, J. Food Eng. 127 (2014) 67–74, https://doi.org/10.1016/j.jfoodeng.2013.11.023.
[38] E. Högg, C. Rauh, Towards a better understanding of texturization during high-moisture extrusion (HME)—part I: Modeling the Texturability of plant-based proteins, Foods 12 (10) (2023) 1955, https://doi.org/10.3390/foods12101955.
[39] B.L. Mojet, S.D. Ebbesen, L. Lefferts, Light at the interface: the potential of attenuated total reflection infrared spectroscopy for understanding heterogeneous catalysis in water, Chem. Soc. Rev. 39 (12) (2010) 4643, https://doi.org/10.1039/c0cs00014k.
[40] D.J. Belton, R. Plowright, D.L. Kaplan, C.C. Perry, A robust spectroscopic method for the determination of protein conformational composition – application to the annealing of silk, Acta Biomater. 73 (2018) 355–364, https://doi.org/10.1016/j.actbio.2018.03.058.
[41] M.G. Bridelli, Fourier Transform Infrared Spectroscopy in the Study of Hydrated Biological Macromolecules, in: In Fourier Transforms - High-tech Application and Current Trends, InTech, 2017, https://doi.org/10.5772/66576.
[42] Y. Shen, X. Tang, Y. Li, Drying methods affect physicochemical and functional properties of quinoa protein isolate, Food Chem. 339 (2021) 127823, https://doi.org/10.1016/j.foodchem.2020.127823.
[43] W.K. Surewicz, H.H. Mantsch, New insight into protein secondary structure from resolution-enhanced infrared spectra, Biochim. Biophys. Acta Protein Struct. Mol. Enzymol. 952 (1988) 115–130, https://doi.org/10.1016/0167-4838(88)90107-0.
[44] V.A. Lórenz-Fonfría, J. Villaverde, E. Padrós, Fourier deconvolution in non-self-deconvolving conditions. Effective narrowing, signal-to-noise degradation, and curve fitting, Appl. Spectrosc. 56 (2) (2002) 232–242, https://doi.org/10.1366/0003702021954494.
[45] de Aragão de B.J.G., Y. Messaddeq, Peak separation by derivative spectroscopy applied to ftir analysis of hydrolized silica, J. Braz. Chem. Soc. 19 (8) (2008) 1582–1594, https://doi.org/10.1590/S0103-50532008000800019.
[46] F. Van Van Breugel, J.N. Kutz, B.W. Brunton, Numerical differentiation of Noisy data: a unifying multi-objective optimization framework, IEEE Access 8 (2020) 196865–196877, https://doi.org/10.1109/ACCESS.2020.3034077.
[47] A. Martínez-Velasco, C. Lobato-Calleros, B.E. Hernández-Rodríguez, A. Román-Guerrero, J. Alvarez-Ramirez, E.J. Vernon-Carter, High intensity ultrasound treatment of faba bean (Vicia faba L.) protein: effect on surface properties, foaming ability and structural changes, Ultrason. Sonochem. 44 (2018) 97–105, https://doi.org/10.1016/j.ultsonch.2018.02.007.
[48] V.A. Lórenz-Fonfría, E. Padrós, The role and selection of the filter function in Fourier self-deconvolution revisited, Appl. Spectrosc. 63 (7) (2009) 791–799, https://doi.org/10.1366/000370209788701161.
[49] F. Nasrollahzadeh, L. Roman, K. Skov, L.M.A. Jakobsen, B.M. Trinh, E. D. Tsochatzis, T. Mekonnen, M. Corredig, J.R. Dutcher, M.M. Martinez, A comparative investigation of seed storage protein fractions: the synergistic impact of molecular properties and composition on anisotropic structuring, Food Hydrocoll. 137 (2023) 108400, https://doi.org/10.1016/j.foodhyd.2022.108400.
[50] G. Ribeiro, M.-Y. Piñero, F. Parle, B. Blanco, L. Roman, Optimizing screw speed and barrel temperature for textural and nutritional improvement of soy-based high-moisture extrudates, Foods 13 (11) (2024) 1748, https://doi.org/10.3390/foods13111748.
[51] M. Fevzioglu, O.K. Ozturk, B.R. Hamaker, O.H. Campanella, Quantitative approach to study secondary structure of proteins by FT-IR spectroscopy, using a model wheat gluten system, Int. J. Biol. Macromol. 164 (2020) 2753–2760, https://doi.org/10.1016/j.ijbiomac.2020.07.299.
[52] P.J. Flory, Statistical mechanics of chain molecules, 1969. ISBN 0-470-26495-0; reissued 1989, ISBN 1-56990-019-1.
[53] M. Conradi, H. Christiansen, S. Majumder, F. Müller, W. Janke, Nonequilibrium dynamics of the Helix-coil transition in polyalanine, Preprint, https://arxiv.org/html/2508.15547v, 2025.
[54] L.J. Smith, K.M. Fiebig, H. Schwalbe, C.M. Dobson, The concept of a random coil: residual structure in peptides and denatured proteins, Fold. Des. 1 (5) (1996) R95–R106, https://doi.org/10.1016/s1359-0278(96)00046-6.
[55] Z. Xiao, R. Jiang, J. Huo, H. Wang, H. Li, S. Su, Y. Gao, Y. Duan, Rice bran meat analogs: relationship between extrusion parameters, apparent properties and secondary structures, LWT 163 (2022) 113535, https://doi.org/10.1016/j.lwt.2022.113535.
[56] X. Li, S. Da, C. Li, F. Xue, T. Zang, Effects of high-intensity ultrasound pretreatment with different levels of power output on the antioxidant properties of alcalase hydrolyzates from quinoa (Chenopodium quinoa Willd.) protein isolate, Cereal Chem. 95 (4) (2018) 518–526, https://doi.org/10.1002/cche.10055.
[57] B. Shivu, S. Seshadri, J. Li, K.A. Oberg, V.N. Uversky, A.L. Fink, Distinct β-sheet structure in protein aggregates determined by ATR–FTIR spectroscopy, Biochemistry 52 (31) (2013) 5176–5183, https://doi.org/10.1021/bi400625v.
[58] B. Mao, J. Singh, S. Hodgkinson, M. Farouk, L. Kaur, Conformational changes and product quality of high-moisture extrudates produced from soy, rice, and pea proteins, Food Hydrocoll. 147 (2024) 109341, https://doi.org/10.1016/j.foodhyd.2023.109341.
[59] A.G. de Brevern, A perspective on the (rise and fall of) protein β-turns, Int. J. Mol. Sci. 23 (20) (2022) 12314, https://doi.org/10.3390/ijms232012314.
[60] F. Wang, Y. Gao, X. Gu, B. Luan, Y. Zhu, Y. Huang, X. Zhu, High-moisture extrusion cooking on soybean-wheat protein mixtures: effect of sodium alginate/xanthan gum/maltodextrin on promoting a fibrous structure, Front. Nutr. 9 (2023), https://doi.org/10.3389/fnut.2022.1077601.
[61] B. Zhang, X. Kang, Y. Cheng, B. Cui, A.M. Abd El-Aty, Impact of high moisture contents on the structure and functional properties of pea protein isolate during extrusion, Food Hydrocoll. 127 (2022) 107508, https://doi.org/10.1016/j.foodhyd.2022.107508.
[62] S.M. Beck, K. Knoerzer, J. Sellahewa, M.A. Emin, J. Arcot, Effect of different heat-treatment times and applied shear on secondary structure, molecular weight distribution, solubility and rheological properties of pea protein isolate as investigated by capillary rheometry, J. Food Eng. 208 (2017) 66–76, https://doi.org/10.1016/j.jfoodeng.2017.03.016.
[63] C.M. Baronio, H. Li, G. Song, H.T. Pigott Annecke, R. Gustafsson, M. Martínez-Carranza, P. Stenmark, A. Barth, The amide I spectrum of parallel β-sheet proteins. https://www.diva-portal.org/smash/get/diva2:1411242/FULLTEXT01.pdf, 2020.
[64] H. Torii, M. Tasumi, Ab initio molecular orbital study of the amide I vibrational interactions between the peptide groups in di- and tripeptides and considerations on the conformation of the extended helix, J. Raman Spectrosc. 29 (1) (1998) 81–86, https://doi.org/10.1002/(SICI)1097-4555(199801)29:1<81::AID-JRS214>3.0.CO;2-H.
[65] E. Goormaghtigh, J.-M. Ruysschaert, V. Raussens, Evaluation of the information content in infrared spectra for protein secondary structure determination, Biophys. J. 90 (8) (2006) 2946–2957, https://doi.org/10.1529/biophysj.105.072017.
[66] B. Byanju, M.M. Rahman, M.P. Hojilla-Evangelista, B.P. Lamsal, Effect of high-power sonication pretreatment on extraction and some physicochemical properties of proteins from chickpea, kidney bean, and soybean, Int. J. Biol. Macromol. 145 (2020) 712–721, https://doi.org/10.1016/j.ijbiomac.2019.12.118.
[67] G. Pellerin, A. Doyen, Effect of thermal and defatting treatments on the composition, protein profile and structure of house cricket (Acheta domesticus) protein extracts, Food Chem. 448 (2024) 139149, https://doi.org/10.1016/j.foodchem.2024.139149.
[68] A. Schwaighofer, H. Anderle, M. Lemmerer, Comparison of spectroscopic techniques for determination of protein secondary structure, Spectrochimica Acta Part A Mol. Biomol. Spectrosc. 340 (2025) 126345, https://doi.org/10.1016/j.saa.2025.126345.
[69] J. de Boer, E. Capuano, J.G. Kers, A.J. van der Goot, High-moisture extrusion enhances soy protein quality based on in vitro protein digestibility and amino acid scores, Food Res. Int. 211 (2025) 116353, https://doi.org/10.1016/j.foodres.2025.116353.
[70] Z. Öztürk, M. Lille, N. Rosa-Sibakov, N. Sozer, Impact of heat treatment and high moisture extrusion on the in vitro protein digestibility of sunflower and pea protein ingredients, LWT 214 (2024) 117133, https://doi.org/10.1016/j.lwt.2024.117133.
[71] S. Salazar-Villanea, W.H. Hendriks, E.M.A.M. Bruininx, H. Gruppen, A.F.B. van der Poel, Protein structural changes during processing of vegetable feed ingredients used in swine diets: implications for nutritional value, Nutr. Res. Rev. 29 (1) (2016) 126–141, https://doi.org/10.1017/S0954422416000056.
[72] G.-H. Ryu, Extrusion cooking of high-moisture meat analogues, in: Extrusion Cooking, Elsevier, 2020, pp. 205–224, https://doi.org/10.1016/B978-0-12-815360-4.00007-9.

[73] C.J.R. Verbeek, L.E. van den Berg, Extrusion processing and properties of protein-based thermoplastics, Macromol. Mater. Eng. 295 (1) (2010) 10–21, https://doi.org/10.1002/mame.200900167.
[74] P. Wittek, N. Zeiler, H.P. Karbstein, M.A. Emin, High moisture extrusion of soy protein: investigations on the formation of anisotropic product structure, Foods 10 (1) (2021) 102, https://doi.org/10.3390/foods10010102.
[75] J.L. Sandoval Murillo, R. Osen, S. Hiermaier, G. Ganzenmüller, Towards understanding the mechanism of fibrous texture formation during high-moisture extrusion of meat substitutes, J. Food Eng. 242 (2019) 8–20, https://doi.org/10.1016/j.jfoodeng.2018.08.009.
[76] V.L. Pietsch, J.M. Bühler, H.P. Karbstein, M.A. Emin, High moisture extrusion of soy protein concentrate: influence of thermomechanical treatment on protein-protein interactions and rheological properties, J. Food Eng. 251 (2019) 11–18, https://doi.org/10.1016/j.jfoodeng.2019.01.001.
[77] S. Ilo, R. Schoenlechner, E. Berghofe, Role of lipids in the extrusion cooking processes, Grasas Aceites 51 (1–2) (2000) 97–110, https://doi.org/10.3989/gya.2000.v51.i1-2.410.
[78] J. Zhang, L. Liu, Y. Jiang, F. Shah, Y. Xu, Q. Wang, High-moisture extrusion of peanut protein−/carrageenan/sodium alginate/wheat starch mixtures: effect of different exogenous polysaccharides on the process forming a fibrous structure, Food Hydrocoll. 99 (2020) 105311, https://doi.org/10.1016/j.foodhyd.2019.105311.
[79] P. Guerrero, J.P. Kerry, K. de la Caba, FTIR characterization of protein–polysaccharide interactions in extruded blends, Carbohydr. Polym. 111 (2014) 598–605, https://doi.org/10.1016/j.carbpol.2014.05.005.